Supporting Information

A Three-in-One Strategy Enable Improved Kinetics in LLZTO Solid Electrolyte for Li-CO_2 Batteries with High Energy Efficiency

Zesen Gao[1], Shijie Yang[2], Yan Yang[1], Futing Sun[1], Tianshuo Zhang[1], Yunluo Wang[1], Tianrui Zhou[1], Lang Tao[1], Hucheng Song[2,*], and Haijie Chen[1,*]

[1]*State Key Laboratory of Advanced Fiber Materials, Institute of Functional Materials, College of Materials Science and Engineering, Donghua University, Shanghai, 201620, People's Republic of China*

[2]*School of Physics, Nanjing University of Aeronautics and Astronautics, Nanjing, 210093, People's Republic of China*

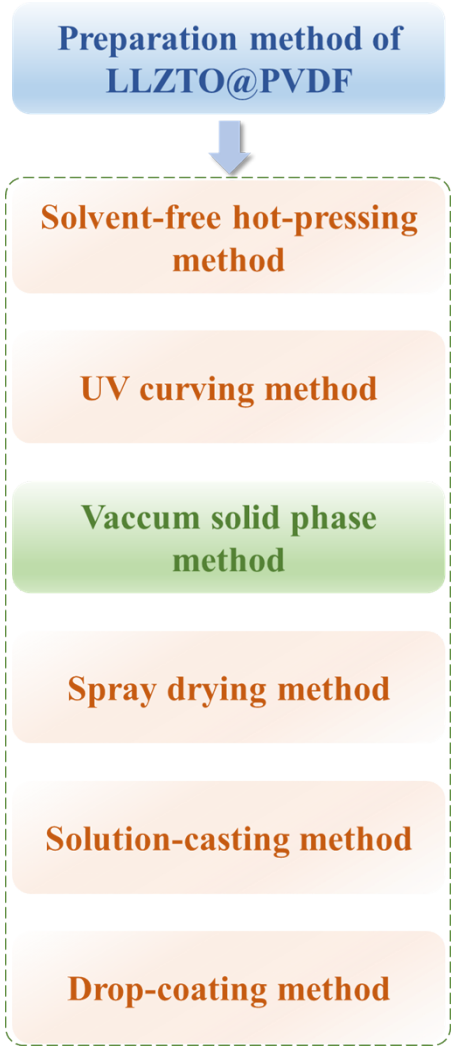

Figure S1. Preparation method of LLZTO@PVDF composite solid-state electrolyte.

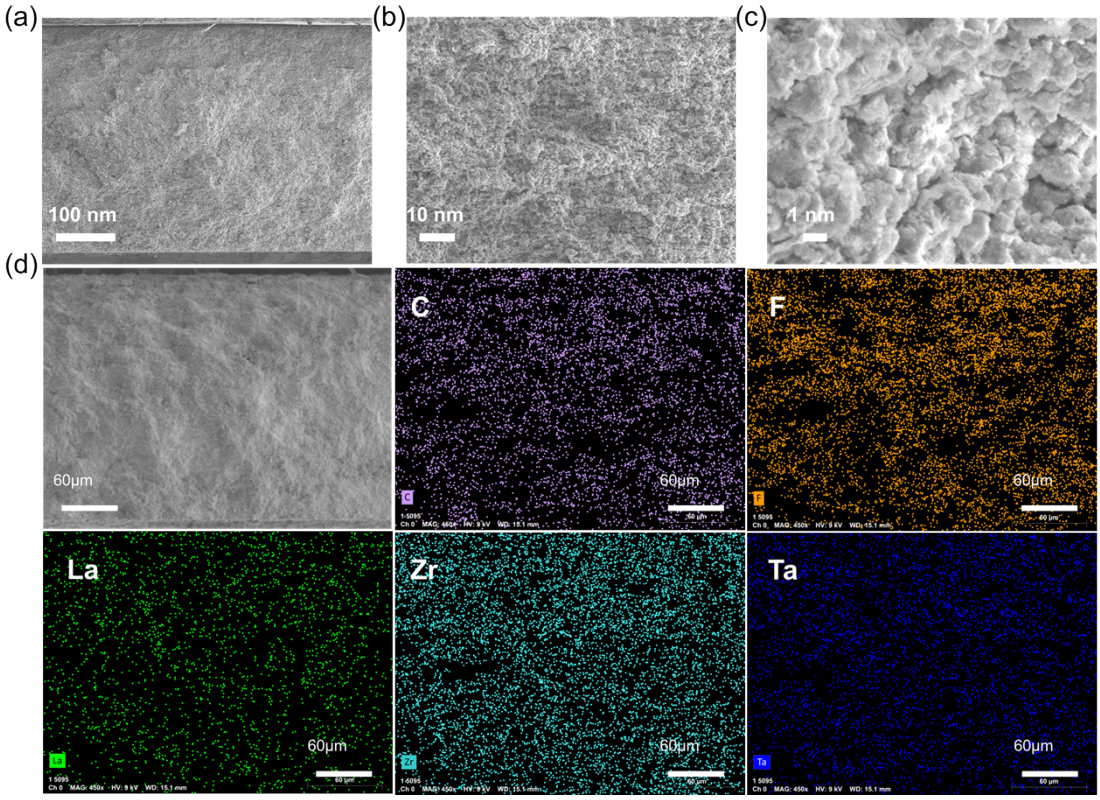

Figure S2. The cross-section morphology of LZPF solid electrolyte pellet under scanning electron microscope.

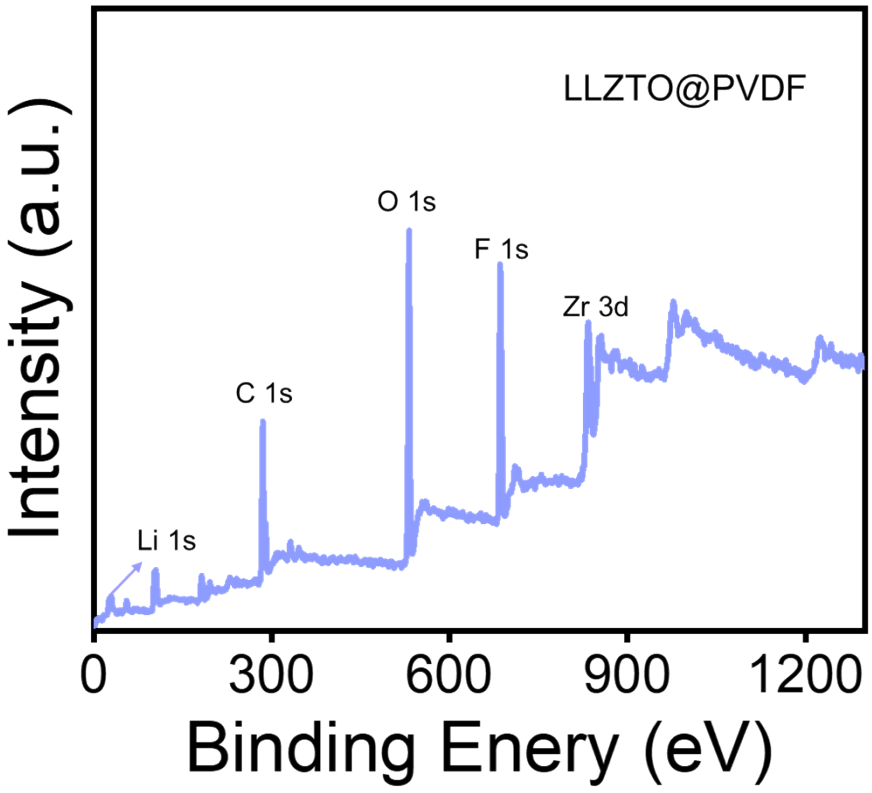

Figure S3. XPS full spectrum of LLZTO@PVDF.

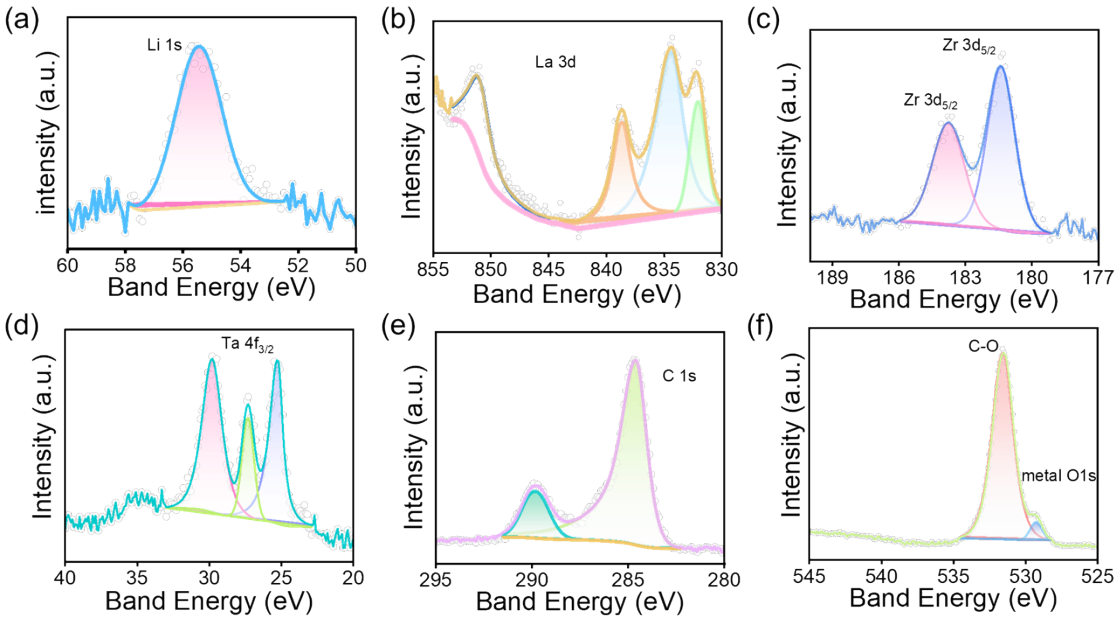

Figure S4. XPS spectra of LLZTO@PVDF solid electrolyte after charging. (a) XPS spectra of Li 1s. (b) XPS spectra of La 3d. (c) XPS spectra of Zr 3d. (d) XPS spectra of Ta 4f. (e) XPS spectra of C 1s. (f) XPS spectra of O 1s.

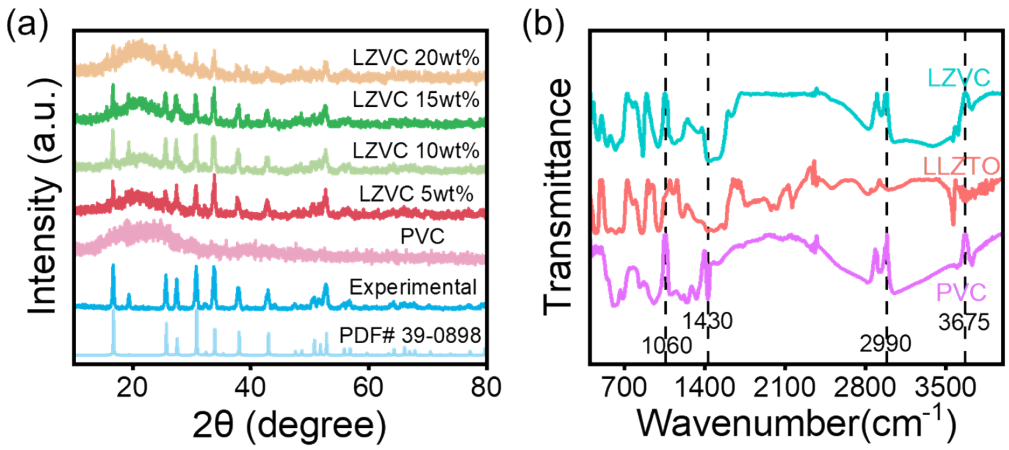

Figure S5. (a) Powder X-ray diffraction patterns of LLZTO@PVC solid electrolytes with different contents of PVC. (b) Fourier transform infrared spectroscopy of LZVC solid electrolytes with different contents of PVC.

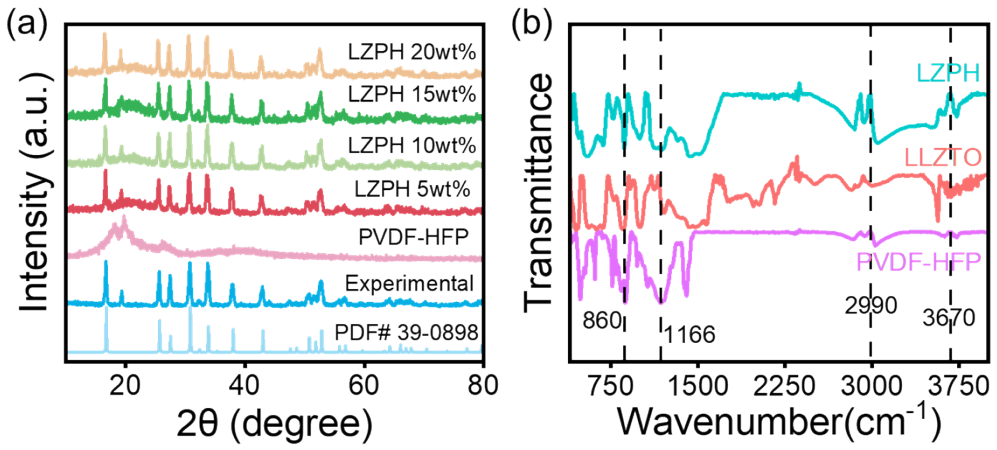

Figure S6. (a) Powder X-ray diffraction patterns of LLZTO@PVDF-HFP solid electrolytes with different contents of PVDF-HFP. (b) Fourier transform infrared spectroscopy of LZPH solid electrolytes with different contents of PVDF-HFP.

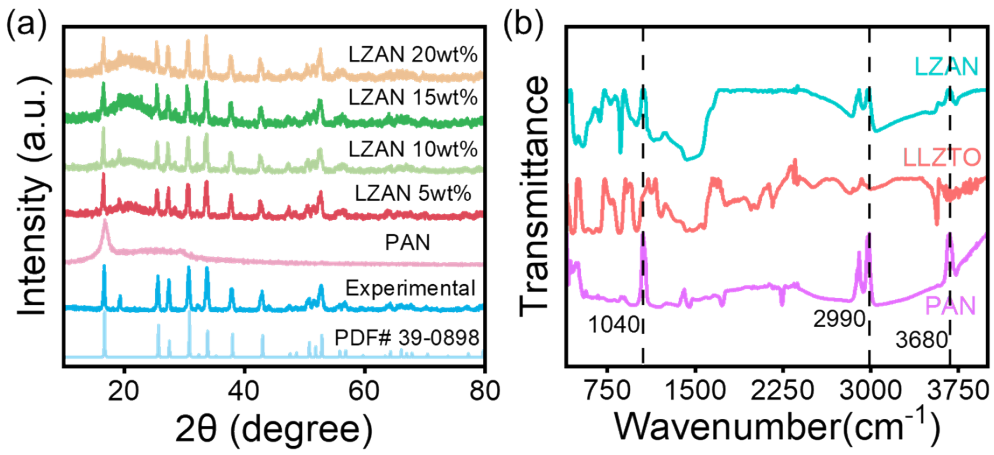

Figure S7. (a) Powder X-ray diffraction patterns of LLZTO@PAN solid electrolytes with different contents of PAN. (b) Fourier transform infrared spectroscopy of LZAN solid electrolytes with different contents of PAN.

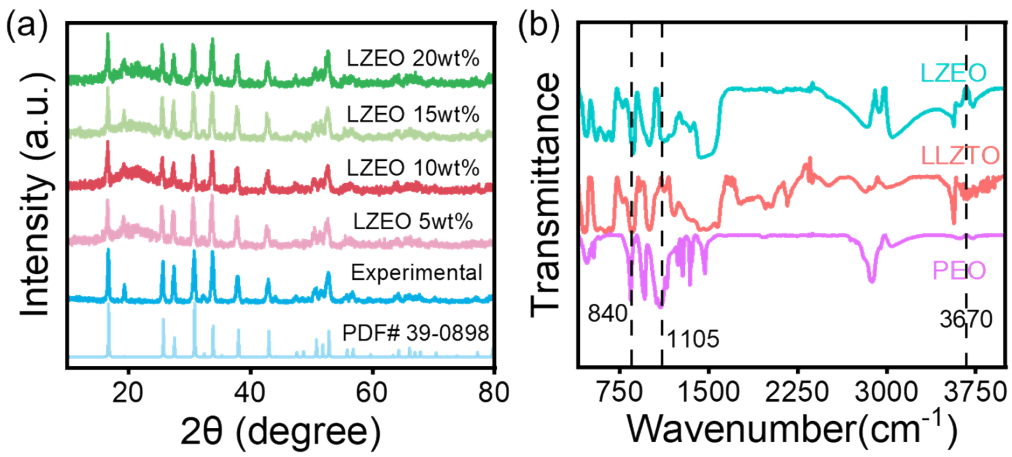

Figure S8. (a) Powder X-ray diffraction patterns of LLZTO@PEO solid electrolytes with different contents of PEO. (b) Fourier transform infrared spectroscopy of LZEO solid electrolytes with different contents of PEO.

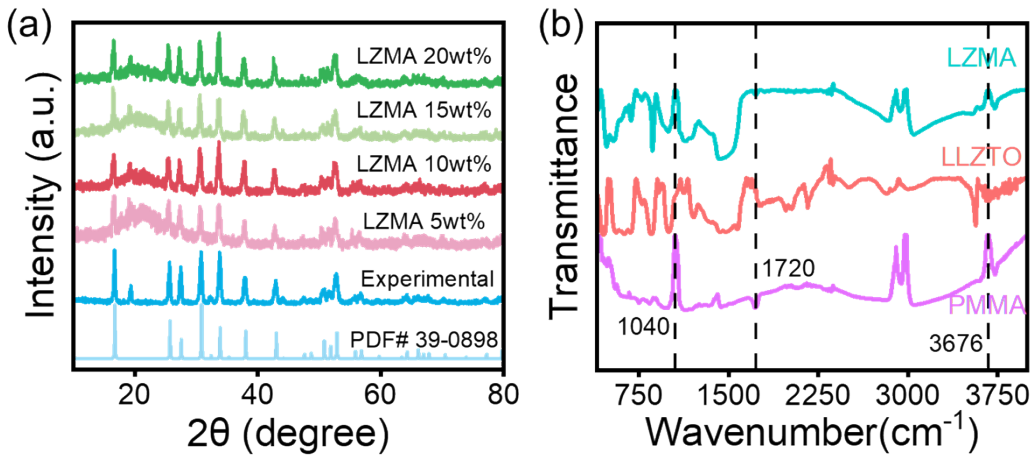

Figure S9. (a) Powder X-ray diffraction patterns of LLZTO@PMMA solid electrolytes with different contents of PMMA. (b) Fourier transform infrared spectroscopy of LZMA solid electrolytes with different contents of PMMA.

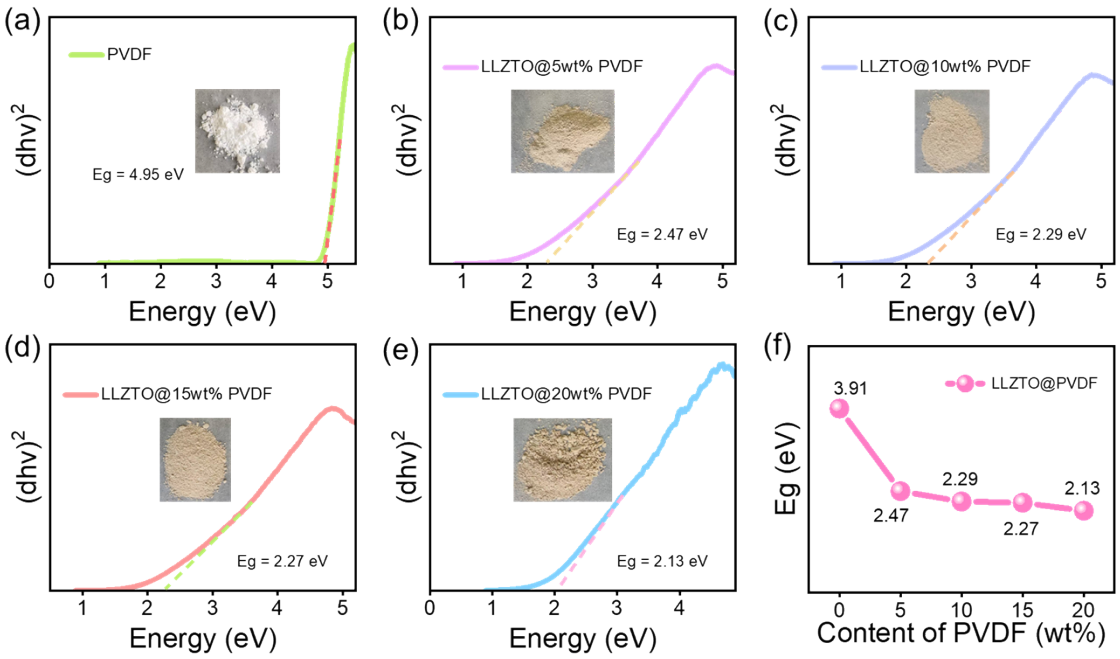

Figure S10. The band gap of (a) PVDF (b) LLZTO@5wt% PVDF (c) LLZTO@10wt% PVDF (d) LLZTO@15wt% PVDF (e) LLZTO@20wt% PVDF obtained from UV-Vis dichroic absorption spectrum. (f) The change curve of LLZTO@PVDF band gap with PVDF content.

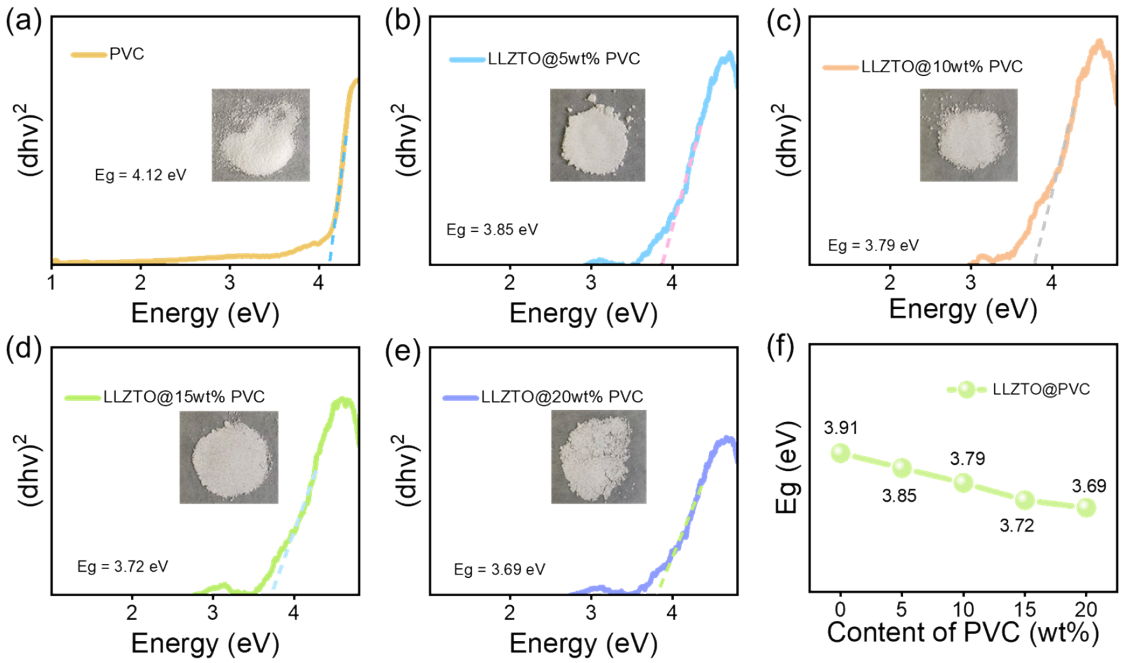

Figure S11. The band gap of (a) PVC (b) LLZTO@5wt% PVC (c) LLZTO@10wt% PVC (d) LLZTO@15wt% PVC (e) LLZTO@20wt% PVC obtained from UV-Vis dichroic absorption spectrum. (f) The change curve of LLZTO@PVC band gap with PVC content.

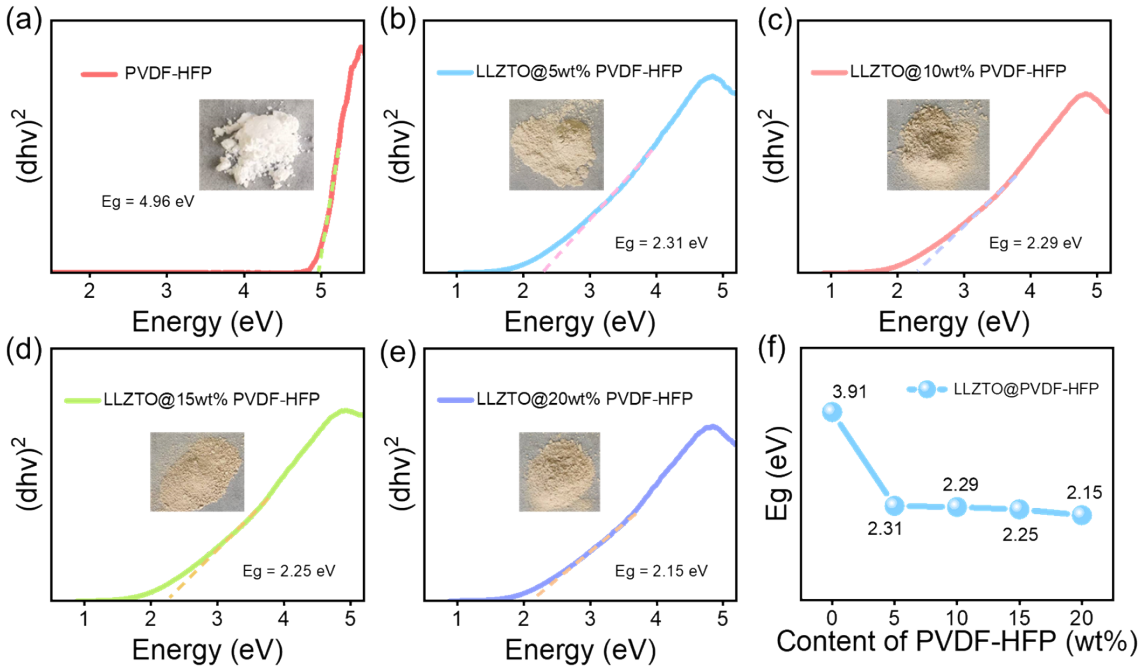

Figure S12. The band gap of (a) PVDF-HFP (b) LLZTO@5wt% PVDF-HFP (c) LLZTO@10wt% PVDF-HFP (d) LLZTO@15wt% PVDF-HFP (e) LLZTO@20wt% PVDF-HFP obtained from UV-Vis dichroic absorption spectrum. (f) The change curve of LLZTO@ PVDF-HFP band gap with PVDF-HFP content.

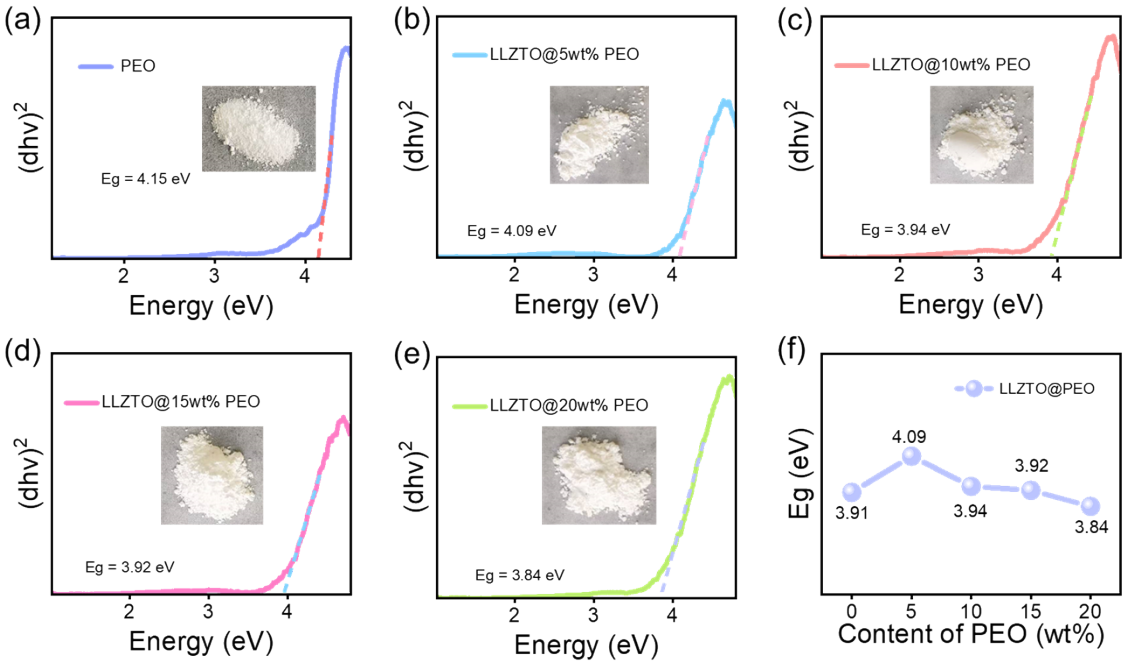

Figure S13. The band gap of (a) PEO (b) LLZTO@5wt% PEO (c) LLZTO@10wt% PEO (d) LLZTO@15wt% PEO (e) LLZTO@20wt% PEO obtained from UV-Vis dichroic absorption spectrum. (f) The change curve of LLZTO@ PEO band gap with PEO content.

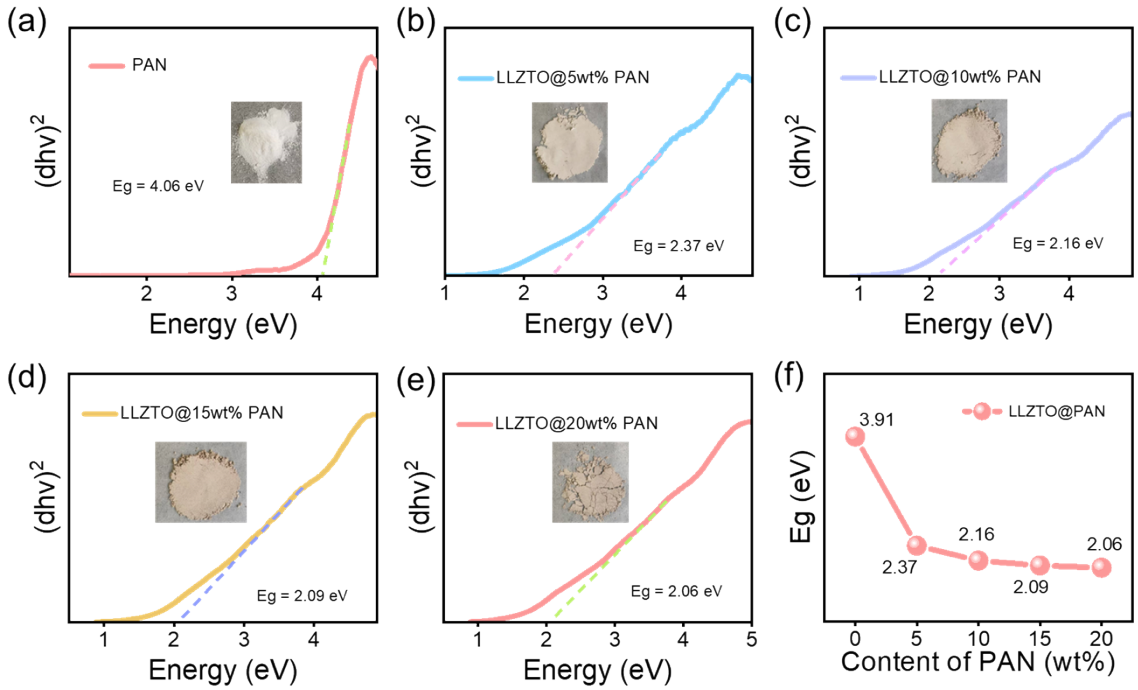

Figure S14. The band gap of (a) PAN (b) LLZTO@5wt% PAN (c) LLZTO@10wt% PAN (d) LLZTO@15wt% PAN (e) LLZTO@20wt% PAN obtained from UV-Vis dichroic absorption spectrum. (f) The change curve of LLZTO@ PAN band gap with PAN content.

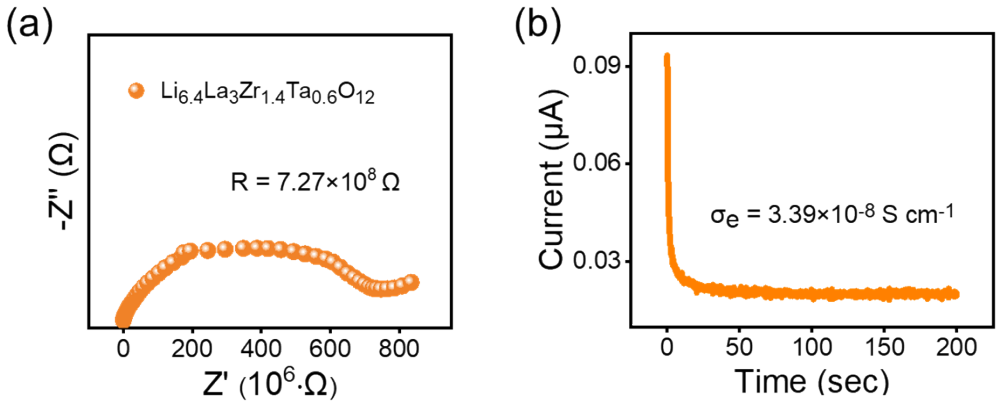

Figure S15. (a) Electrochemical impedance spectroscopy of LLZTO solid electrolyte at room temperature. (b) i-t curves of LLZTO solid electrolyte at room temperature.

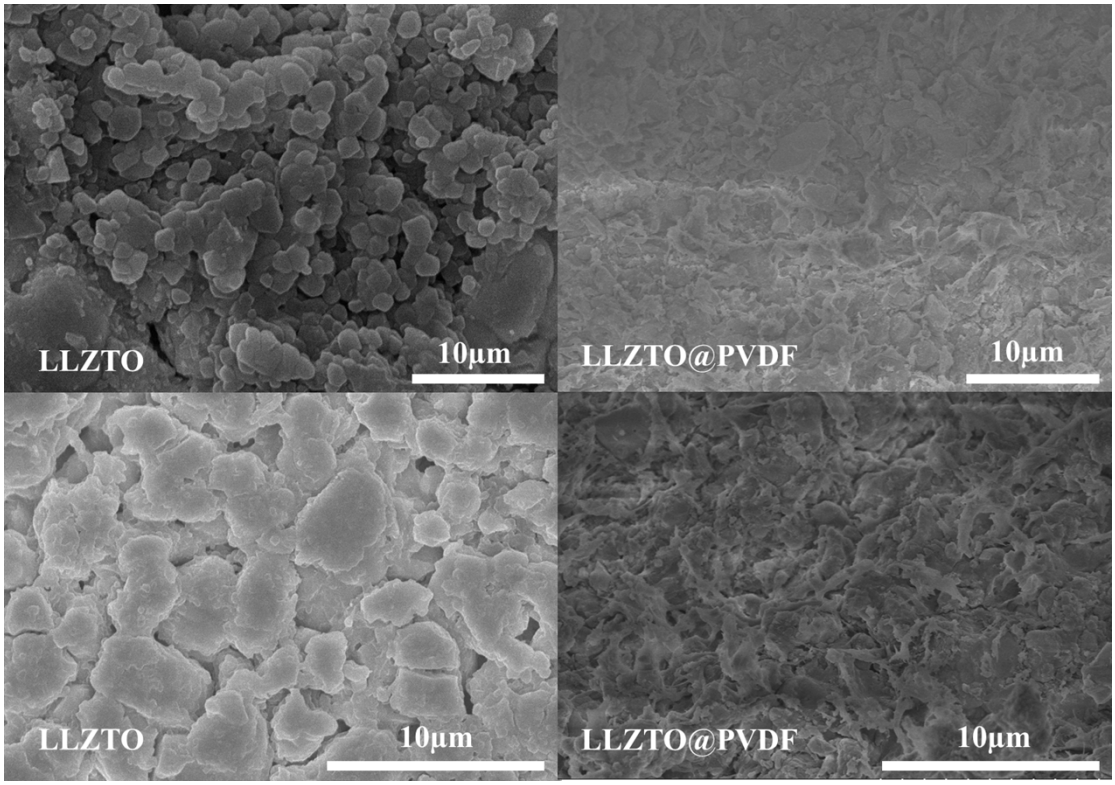

Figure S16. The cross-section morphology of LLZTO and LLZTO@PVDF solid electrolyte pellet under scanning electron microscope.

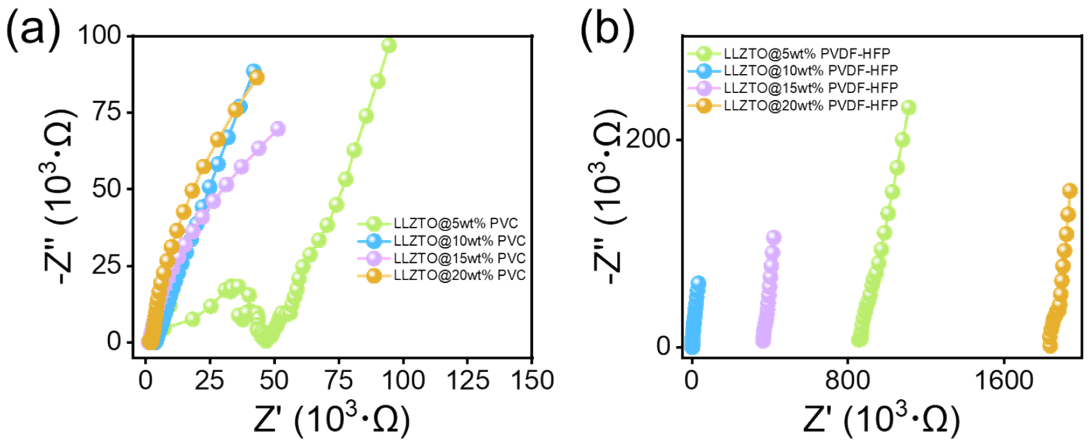

Figure S17. (a) Electrochemical impedance spectroscopy of LLZTO solid electrolyte with different content of PVC (5wt% – 30wt%) at room temperature. (b) Electrochemical impedance spectroscopy of LLZTO solid electrolyte with different content of PVDF-HFP (5wt% – 30wt%) at room temperature.

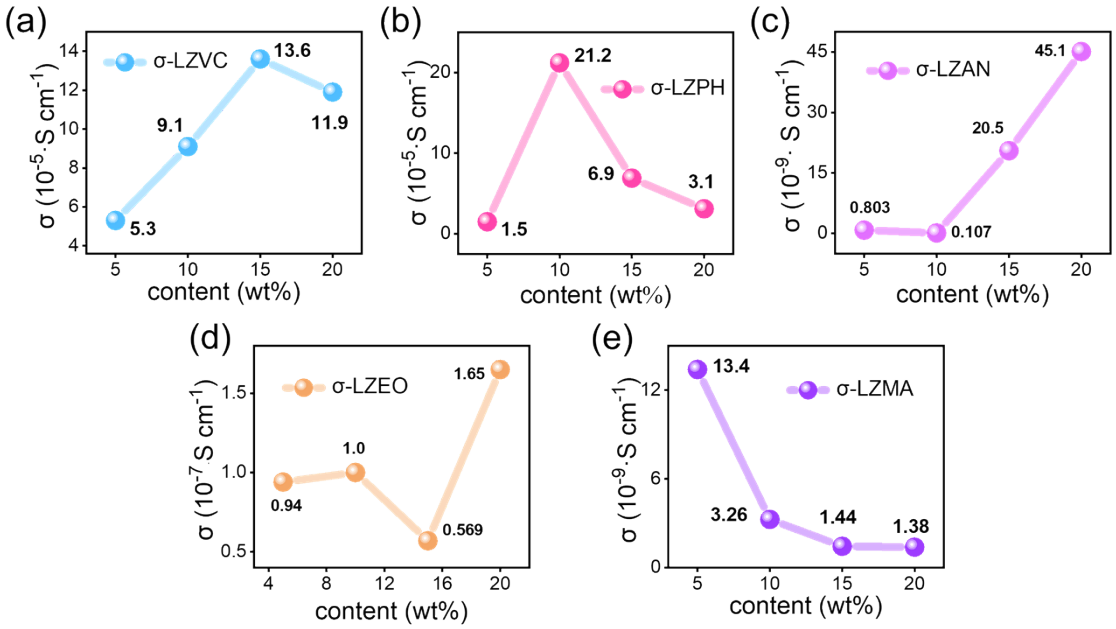

Figure S18. (a) Ionic conductivity change curves of LLZTO solid electrolytes with different contents of PAN (5wt% – 20wt%) compounded at room temperature. (b) Ionic conductivity change curves of LLZTO solid electrolytes with different contents of PEO (5wt% - 20wt%) compounded at room temperature. (c) LLZTO solid electrolytes with different contents of PMMA (5wt% – 20wt%) compounded at room temperature Ionic conductivity change curve of solid-state electrolyte. (d) Ionic conductivity change curve of LLZTO solid state electrolyte compounded with different content of PVC (5wt% – 20wt%) at room temperature. (e) Ionic conductivity change curve of LLZTO solid state electrolyte compounded with different content of PVDF-HFP (5wt% – 20wt%) at room temperature.

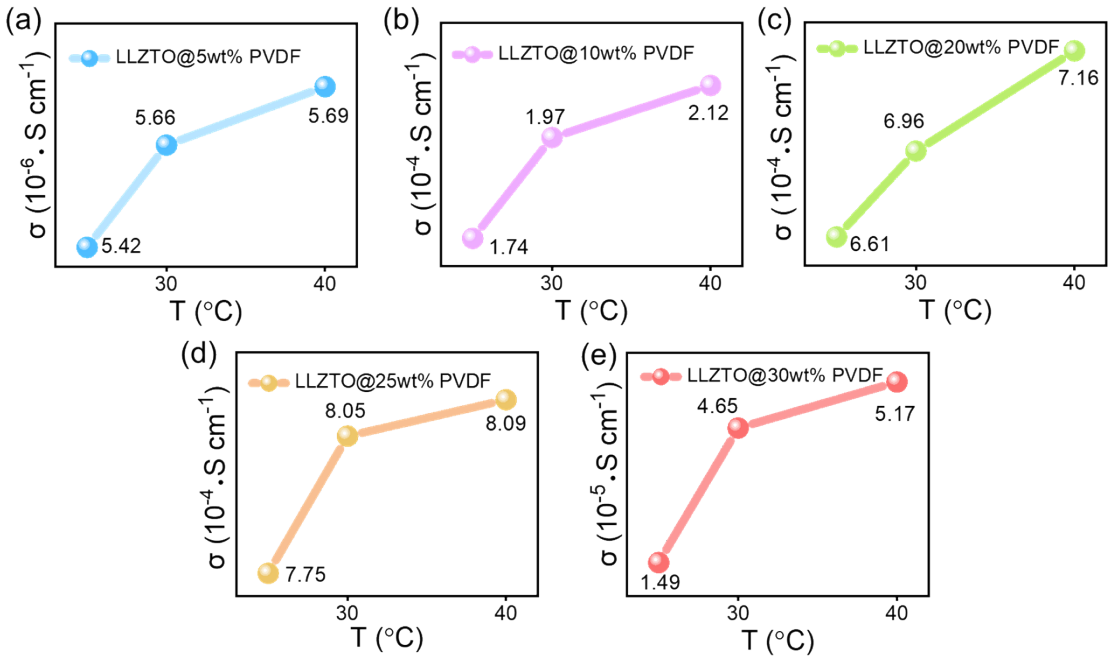

Figure S19. (a)The ionic conductivity curve of LLZTO@ 5wt%PVDF solid electrolyte at different temperatures. (b)The ionic conductivity curve of LLZTO@ 10wt%PVDF solid electrolyte at different temperatures. (c)The ionic conductivity curve of LLZTO@ 20wt%PVDF solid electrolyte at different temperatures. (d)The ionic conductivity curve of LLZTO@ 25wt%PVDF solid electrolyte at different temperatures. (e)The ionic conductivity curve of LLZTO@ 30wt%PVDF solid electrolyte at different temperatures.

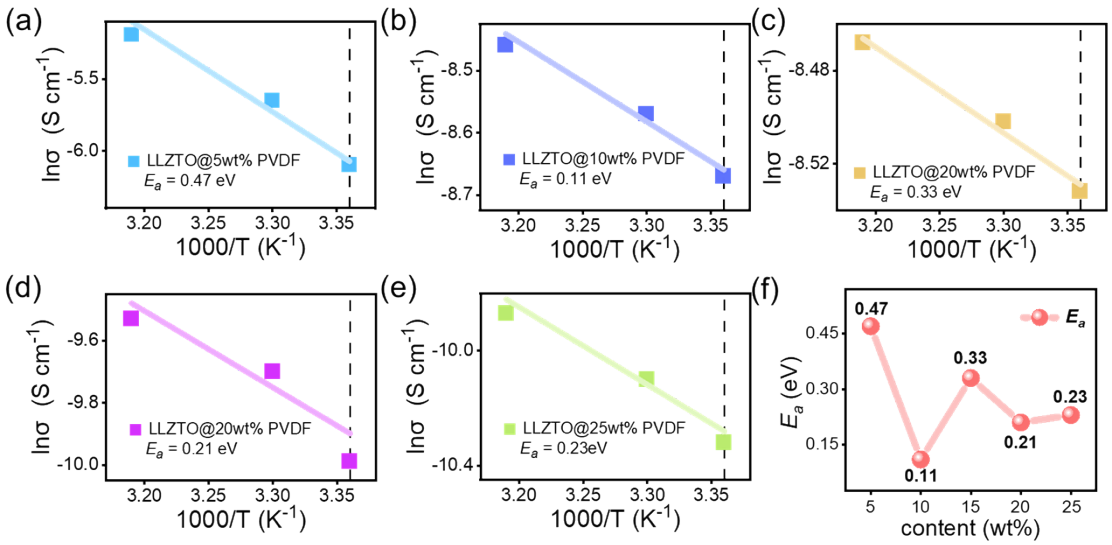

Figure S20. (a) Activation energy of LLZTO@5wt% PVDF solid electrolyte. (b) Activation energy of LLZTO. @ 10wt%PVDF solid electrolyte. (c) Activation energy of LLZTO@15wt% PVDF solid electrolyte. (d) Activation energy of LLZTO@ 20wt% PVDF solid electrolyte. (e) Activation energy of LLZTO@25wt% PVDF solid electrolyte. (f) Activation energy change curve of LLZTO solid electrolyte with different content of PVDF (5wt% – 25wt%).

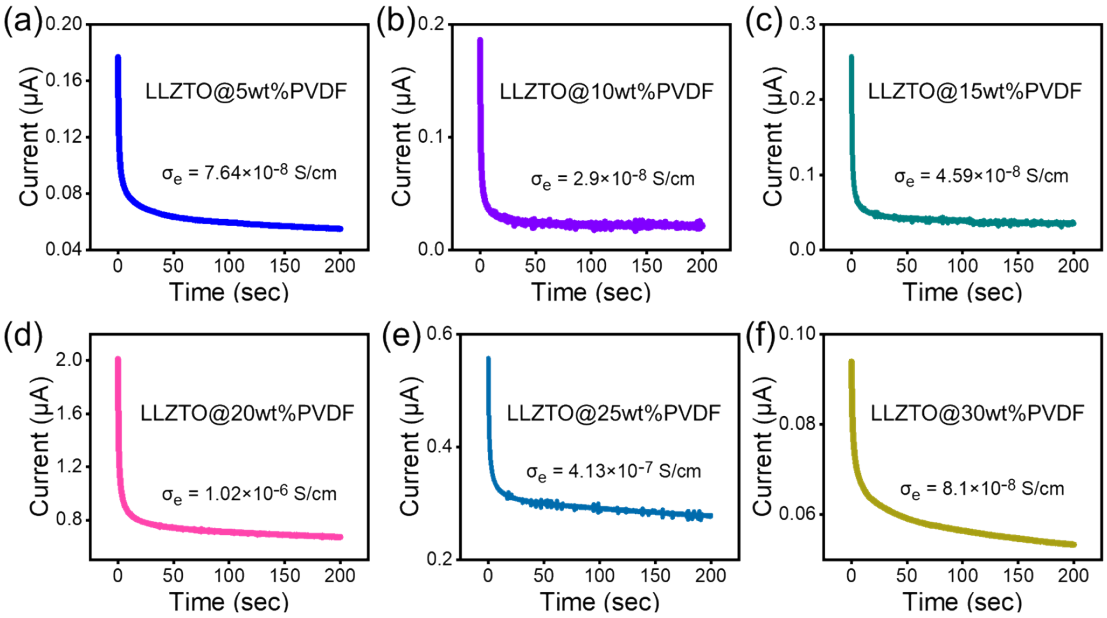

Figure S21. (a) The electronic conductivity of LLZTO@5wt% PVDF solid electrolyte was measured using a double-blocking electrode cell at room temperature. (b) The electronic conductivity of LLZTO@10wt% PVDF solid electrolyte was measured using a double-blocking electrode cell. (c) The electronic conductivity of LLZTO@15wt% PVDF solid electrolyte was measured using a double-blocking electrode cell. (d) The electronic conductivity of LLZTO@20wt%PVDF solid electrolyte was measured using a double-blocking electrode cell. (e) The electronic conductivity of LLZTO@25wt %PVDF solid electrolyte was measured using a double-blocking electrode cell (f) The electronic conductivity of LLZTO@30wt% PVDF solid electrolyte was measured using a double-blocking electrode cell.

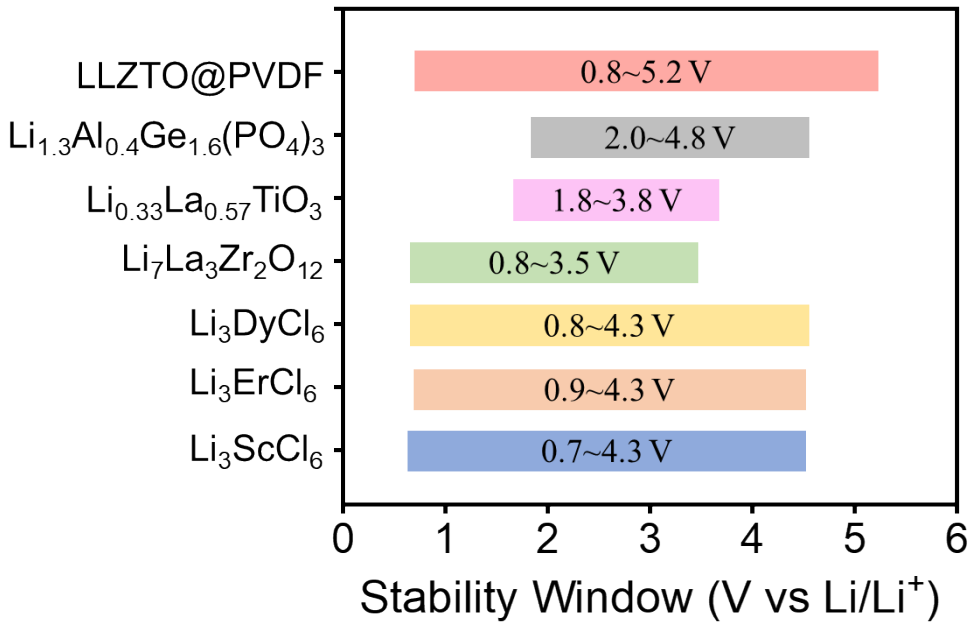

Figure S22. Comparison of electrochemical windows for some halide, oxide and LLZTO@PVDF solid state electrolytes.

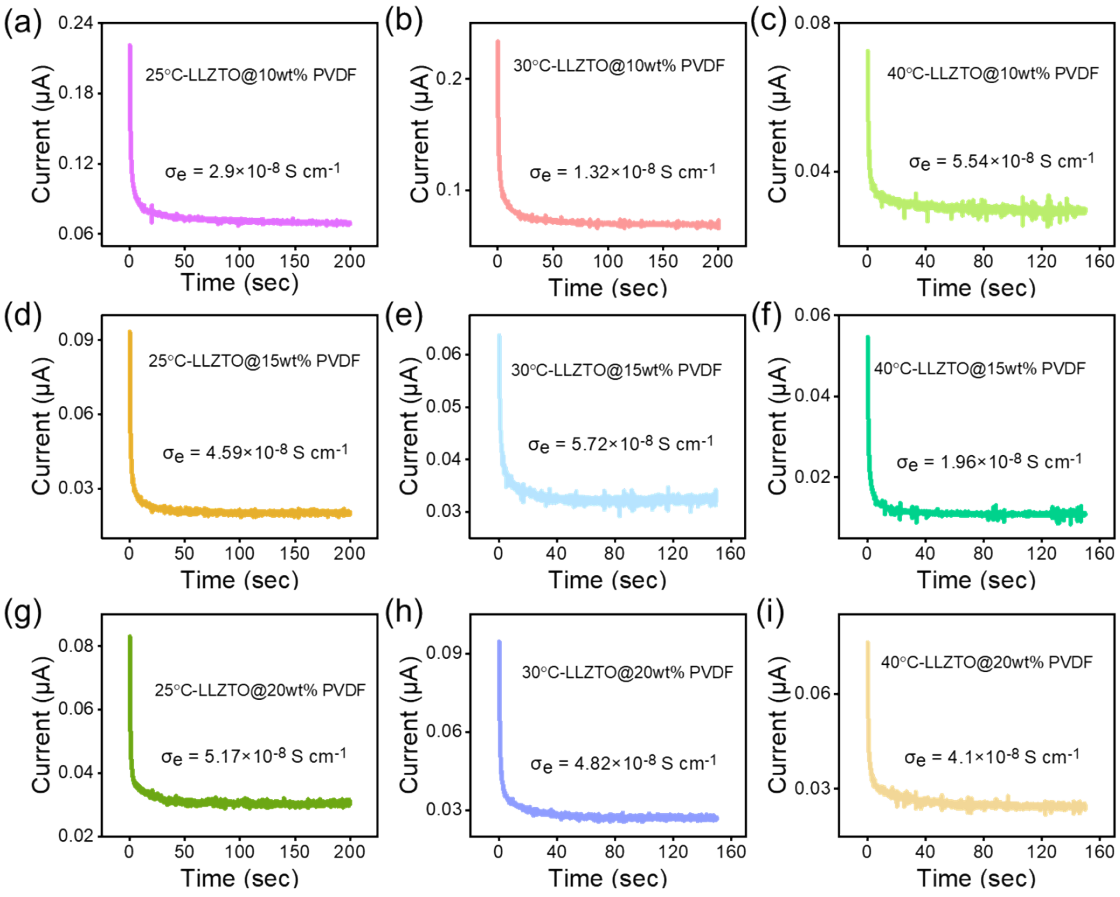

Figure S23. (a) The electronic conductivity of LLZTO@10wt% PVDF solid electrolyte at room temperature. (b) The electronic conductivity of LLZTO@10wt% PVDF solid electrolyte at 30 ℃. (c) The electronic conductivity of LLZTO@10wt% PVDF solid electrolyte at 40 ℃. (d) The electronic conductivity of LLZTO@15wt% PVDF solid electrolyte at room temperature. (e) The electronic conductivity of LLZTO@15wt% PVDF solid electrolyte at 30 ℃. (f) The electronic conductivity of LLZTO@15wt% PVDF solid electrolyte at 40 ℃. (g) The electronic conductivity of LLZTO@20wt% PVDF solid electrolyte at room temperature. (h) The electronic conductivity of LLZTO@20wt% PVDF solid electrolyte at 30 ℃. (i) The electronic conductivity of LLZTO@20wt% PVDF solid electrolyte at 40 ℃.

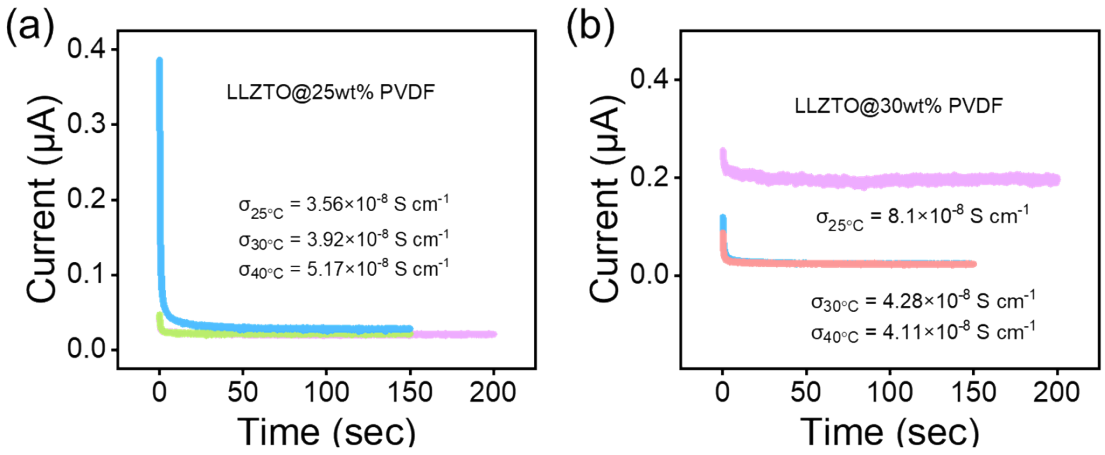

Figure S24. (a) The electronic conductivity of LLZTO@25wt% PVDF solid electrolyte at different temperature (25 ℃, 30 ℃, 40 ℃). (b) The electronic conductivity of LLZTO@25wt% PVDF solid electrolyte at different temperature (25 ℃, 30 ℃, 40 ℃).

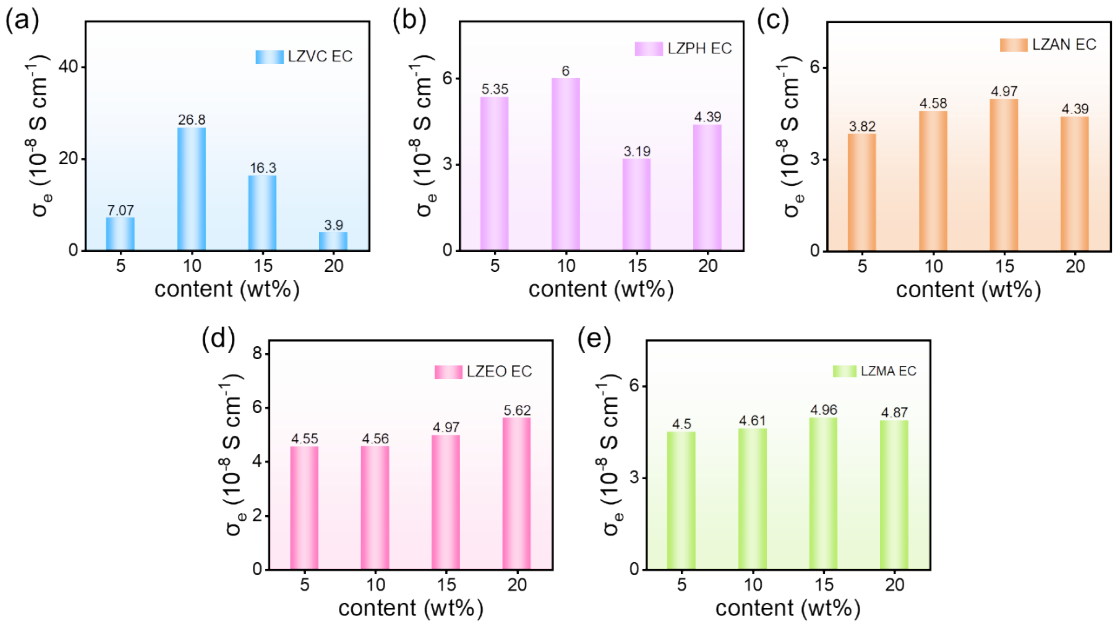

Figure S25. (a) The electronic conductivity curve of LLZTO solid electrolyte with different content of PVC (5wt% – 20wt%) at room temperature. (b) The electronic conductivity curve of LLZTO solid electrolyte with different content of PVDF-HFP (5wt% – 20wt%) at room temperature. (c) The electronic conductivity curve of LLZTO solid electrolyte with different content of PAN (5wt% – 20wt%) at room temperature. (d) The electronic conductivity curve of LLZTO solid electrolyte with different content of PEO (5wt% – 20wt%) at room temperature. (e) The electronic conductivity curve of LLZTO solid electrolyte with different content of PMMA (5wt% – 20wt%) at room temperature.

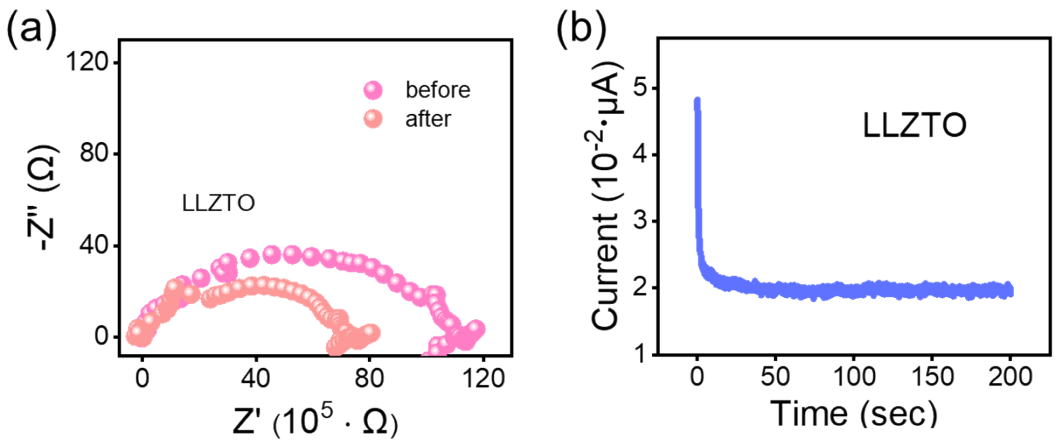

Figure S26. (a) The corresponding Nyquist diagram of LLZTO before and after polarization. (b) The chronoamperometry curve of Li | LLZTO | Li half-cell.

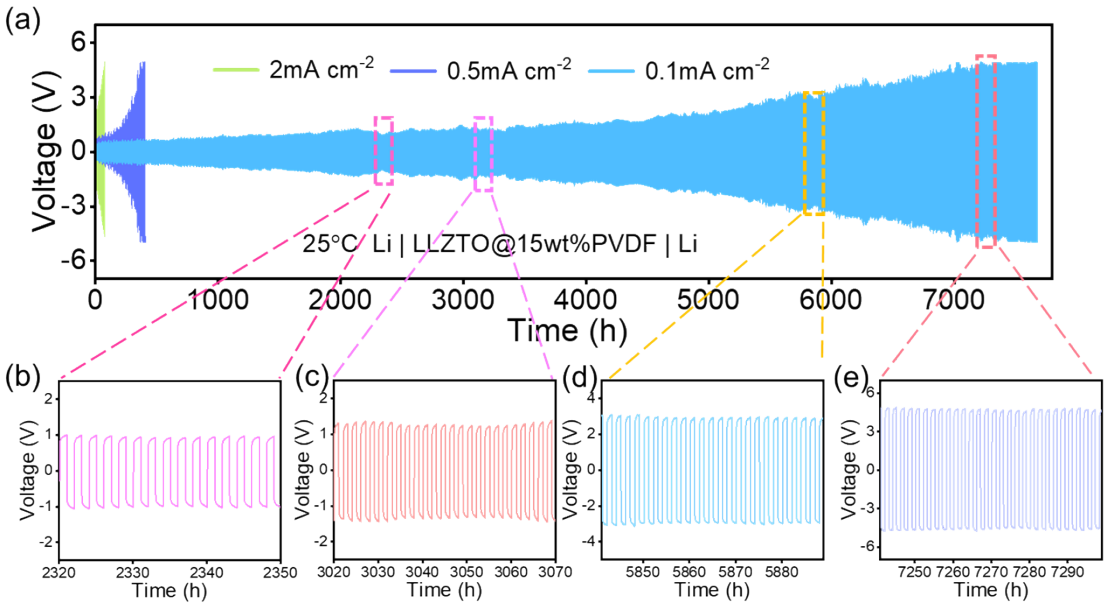

Figure S27. (a) Lithium plating and stripping of Li | LLZTO@15wt% PVDF | Li symmetrical half-cell at 0.1 mA cm^{-2}, 0.5 mA cm^{-2} and 2 mA cm^{-2} current densities at room temperature and the cycle performance of between (b) 2320 h − 2350 h, (c) 3020 h – 3070 h, (d) 5840 h – 5890 h and (e) 7240 h – 7300 h.